Article

Source of Rate Acceleration for Carbocation Cyclization in Biomimetic Supramolecular Cages

Quynh Nhu N. Nguyen,[⊥] Kay T. Xia,[⊥] Yue Zhang,[⊥] Nanhao Chen,[⊥] Mariko Morimoto,[⊥] Xiaokun Pei, Yang Ha, Jinghua Guo, Wanli Yang, Lee-Ping Wang, Robert G. Bergman,* Kenneth N. Raymond,* F. Dean Toste,* and Dean J. Tantillo*

ACCESS | 📊 Metrics & More | 📖 Article Recommendations | 🗒️ Supporting Information

ABSTRACT: The results of quantum chemical and molecular dynamics calculations reveal that polyanionic gallium-based cages accelerate cyclization reactions of pentadienyl alcohols as a result of substrate cage interactions, preferential binding of reactive conformations of substrate/H_3O^+ pairs, and increased substrate basicity. However, the increase in basicity dominates. Experimental structure−activity relationship studies in which the metal vertices and overall charge of the cage are varied confirm the model derived *via* calculations.

$Ga_4L_6^{12-}$

elucidating the origins of rate enhancement
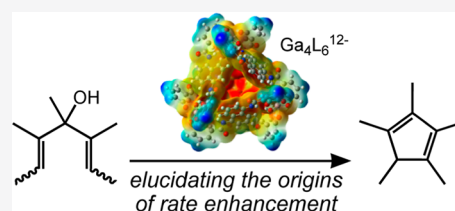
INTRODUCTION

Carbocations are involved as intermediates in catalytic reactions accomplished by both synthetic chemists and biological systems. The latter are most prominently found in the realm of terpene biosynthesis, where terpene synthase enzymes generate carbocations in productive conformations, allowing them to rearrange while protecting them from premature deprotonation or addition by nucleophiles and allowing them to be deprotonated at specific positions (Scheme 1, top, OPP = diphosphate).[1] Synthetic chemists have developed systems that mimic these characteristics.[2,3] In both the synthetic and biosynthetic realms, however, the relative importance of each step in the reaction mechanism is still up for debate. Extensive computational work has targeted this issue for terpene synthases,[1c,d,4] but much less attention has been afforded to synthetic systems.[2,3,5]

Here, we describe molecular dynamics (MD) and quantum chemical computations on a four-electron electrocyclization of pentadienyl carbocations promoted by the tetrahedral Ga_4L_6 cage studied by Raymond, Bergman, Toste, and co-workers (Scheme 1, bottom).[2] The cyclization of dienol **1** (multiple geometric isomers have been examined; only one is shown) typically requires strong Lewis or Bronsted acids in bulk solution to promote protonation of oxygen and generate a pentadienyl carbocation intermediate (**2**), which then undergoes a four-electron electrocyclic ring closure. Under Ga_4L_6-catalyzed conditions, the hydrophobic substrate **1** is first reversibly bound in the naphthalene-walled host cavity, which enables protonation of the alcohol despite the basic aqueous medium outside the host. The substrate ionizes to release water before undergoing four-electron electrocyclization (associated with the highest energy transition state along the reaction coordinate), followed by proton loss to generate the cyclopentadiene product **3**. Due to the similar association

constants of the product (**3**) and substrate (**1**), excess maleimide was added to trap the product as the Diels−Alder adduct **4**, which no longer is encapsulated by the host.

Our results indicate the essential role of the catalyst cage in promoting carbocation formation primarily *via* leaving group basicity enhancement. We also conducted a comprehensive experimental study to validate the model derived from calculations and determine the contribution of the metal vertices to supramolecular catalytic activity. We found that when the overall charge of the host was held constant, changing the metal center had little effect on the host's catalytic performance. Our results provide evidence that supramolecular hosts can tolerate systematic structural modifications without significant loss of catalytic activity.

Computational Methods. Finding a computational approach for modeling such a large system that strikes the right balance between accuracy and efficiency is a challenge. Inspired by the success of Nitschke and co-workers in computing geometries for related cage structures,[6] we first examined the feasibility of employing various density functionals with relatively small basis sets (see the Supporting Information for details). Ultimately, we found that the B3LYP/ 3-21G level of theory,[7] with the LANL2DZ basis set for Ga,[8] provided reasonable results, suitable for surveying a wide range of structures. Optimizing geometries and computing vibrational frequencies with ostensibly "better" levels of theory proved, in our hands, to be impractical at best and intractable
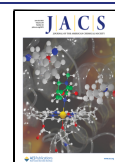
Scheme 1. Top: Typical, Albeit Simple, Terpene Synthase-Promoted Reaction; Bottom: Electrocyclization Promoted by the Ga$_4$L$_6$ Cage; Adapted in Part from Ref 2a
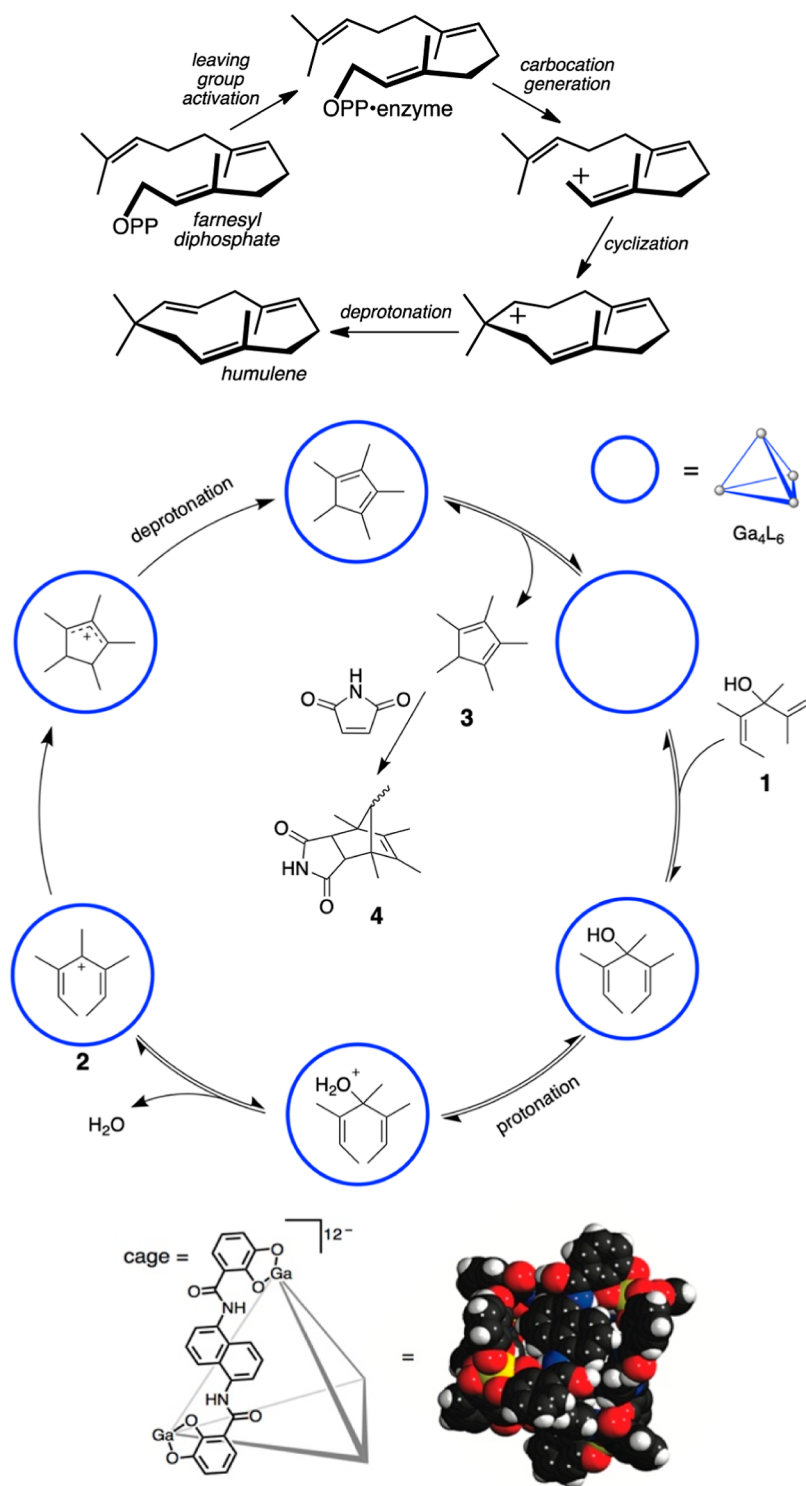
at worst. However, single point energies on B3LYP/3-21G-LANL2DZ geometries with various other functionals and larger basis sets showed that the results described below were not very sensitive to the method used (see the Supporting Information); all led to the same qualitative conclusions. In addition, for substrates in the absence of the cage, we performed optimization and frequency calculations with a variety of methods and larger basis sets; results were again very

similar to those obtained with B3LYP/3-21G (see the Supporting Information). All calculations were conducted using the conductor-like polarizable continuum model (CPCM) for water (the solvent used experimentally),[9] which allowed the cage, which bears a 12$^-$ charge, not to expand significantly beyond its reported crystallographic geometry,[2,10] despite the absence of counterions in these calculations. All

reported energies are free energies at 298 K unless stated otherwise.

In addition to these static calculations, we carried out MD calculations to address conformational and configurational flexibility. These calculations were set up based on the initial quantum mechanics (QM) optimization results. The organic portions of the cage and the ligand molecules were described by the AMBER general force field,[11] and their charges were calculated by the restrained electrostatic potential (RESP) method[12] based on ESP results obtained with HF/6-31G*. Since there are no parameters for Ga or Si in AMBER,[13] we substituted both by Al for our molecular mechanics (MM) calculations (but set the Si charge to 4+). The assumption that any electronic differences aside from the charge between Ga and Si are insignificant is validated experimentally (s). All system preparations were done using the *tleap* program in AMBER 16.[13] In the MM/MD simulations, a multistep strategy was used to heat and equilibrate the system gradually. First, energy minimization was carried out, followed by a 100 ps heating process (*NVT* ensemble). Then, another 100 ps MD simulation was carried out to balance the system (*NPT* ensemble with the help of the Berendsen barostat). Finally, a 50 ns MD simulation (*NVT* ensemble) was carried out. During the heating and equilibrium processes, an extra force was first added to the cage to prevent its contraction, and the SHAKE[14] algorithm was applied to constrain covalent bond lengths involving hydrogen. The cutoff values for short-range electrostatic and van der Waals interactions were set to 12 Å, and the particle-mesh Ewald method was used for long range summation of electrostatic interactions.[15] All MD calculations were carried out using the OpenMM package.[16]

In addition, to estimate energy barriers for leaving group activation and departure, combined QM/MM calculations were carried out using the Q-Chem and AMBER software packages.[13,17] The QM region was set as the guest molecule, one H_3O^+ and two H_2O molecules that engage in hydrogen-bond interactions with H_3O^+. All atoms in the QM region were treated with B3LYP/6-31G*, and all the non-QM atoms were described by the force field mentioned above with a 12 Å cutoff for nonbonded interactions. QM/MM free energy calculations made use of umbrella sampling along with the defined reaction coordinate (*vide infra*) and the weighted histogram analysis method.[18]

RESULTS AND DISCUSSION

Effects of Cage Walls on Cyclization. Raymond, Bergman, and co-workers observed rate accelerations of approximately six orders of magnitude for various isomers of the substrate shown in Scheme 1 in the presence of the cage.[2] Here, we model the substrate with two *E* double bonds. First, we address the issue of whether or not direct interactions with the Ga_4L_6 cage lower the barrier for electrocyclization. The transition state structure (TSS) for electrocyclization in the absence of the cage (but in a water continuum) is shown at the top of Figure 1.[19] A barrier of only ~4 kcal/mol was computed for cyclization from a productive, that is, preorganized, conformer of the reactant. Model calculations (Figure 1, middle and bottom) in the presence of a benzene or naphthalene molecule indicate that the aromatic walls of the cage can provide rate acceleration, although the effect is not large. While the walls interact with the substrate,[2,3d] selective binding of the TSS over the pentadienyl cation intermediate is predicted to amount to <2 kcal/mol, indicating that, at best,
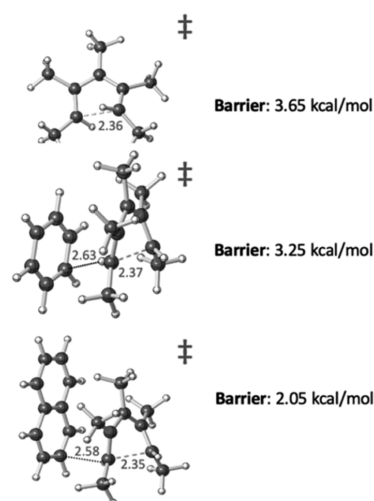

Figure 1. Top to bottom: TSS of the model substrate, TSS with a benzene ring nearby, and TSS with a naphthalene nearby. Each energy barrier was calculated [ωB97XD/6-311+G(d,p)][19] relative to the respective reactant in a similar environment, that is, reactant alone or with benzene or naphthalene in close proximity.

the observed large rate acceleration must originate primarily from another source.

Conformational Preorganization. Another possible contributor to the observed rate acceleration is reactant preorganization; that is, adopting the productive conformation in solution is accompanied by an energy penalty that is "paid" by the catalyst upon binding. Our density functional theory (DFT) calculations suggest, however, that coiled conformers of the substrate, its O-protonated form, and the pentamethyl-pentadienyl cation (where the two end carbons of the pentadienyl system are near each other) are within ~2 kcal/mol of the lowest energy conformer. For the carbocation, this is the lowest energy conformer. Our MD simulations indicate that pentamethylpentadienol in explicit water rapidly explores both extended and compact conformations (Figure 2, top). Upon complexation, it still explores these conformations, although transitions between them are not as smooth (Figure 2, middle). The barrier for transitioning between extended and compact forms inside the cage is estimated to be ~3 kT (roughly 2 kcal/mol at room temperature), while outside the cage, the barrier is close to 0 (energy plot shown in the Supporting Information). In general, as water molecules flow into the cage, the conformation of the guest changes from extended to compact. Overall, there appears to be no significant preorganization induced by the catalyst for the alcohol. Pentamethylpentadienol along with an explicit hydronium ion next to the hydroxyl group of the substrate was also modeled with MD (Figure 2, bottom). In this case, the substrate mainly adopts a relatively compact conformation, suggesting that the alcohol/H_3O^+ pair is preferentially accommodated in orientations productive for the reaction.

Leaving Group Activation—Setting the Stage. That leaves us with leaving group activation. However, an important issue to address in this regard is the number of water molecules contained within the cage, along with any substrates. Warshel and co-workers previously examined the binding of four water molecules plus one H_3O^+ molecule within the same cage examined here.[5a] Based on preliminary DFT calculations, we find that additional water molecules can be encapsulated
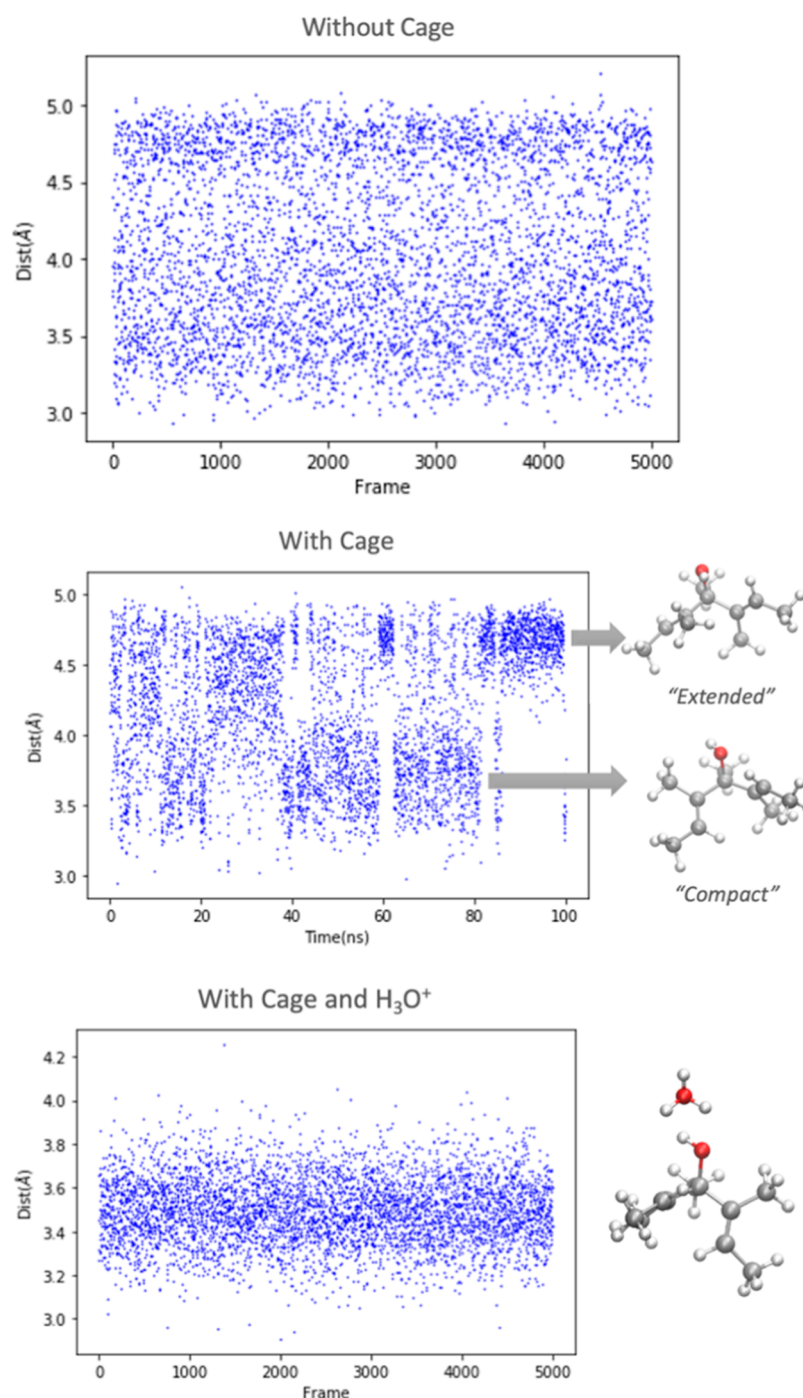
Figure 2. Distance between alkene carbons that will form the new C−C bond vs time during MD simulations. Top: Pentamethylpentadienol in water. Middle: Pentamethylpentadienol in the cage. Bottom: Pentamethylpentadienol with hydronium ion in the cage.

without major distortions to the cage geometry (see the Supporting Information).[20] We also addressed this issue with MD simulations of the cage surrounded by water molecules that can enter and leave its interior. Without the substrate present, a range of 0−16 water molecules were observed inside the cage over the length of the MD simulation, while 10−13 water molecules were the most common number (the cage was restrained to prevent shrinking). Recent experimental evidence pointed to 9 ± 1 water molecules in the cage in question.[5e] With the pentamethylpentadienol substrate present in the cage, 0−4 water molecules were observed in the MD simulation (Figure 3, left, "substrate" bars). When a hydronium ion was

included during MD, 2−5 water molecules were present in the cage along with the substrate (the water count does not include the hydronium ion; Figure 3, left, "substrate + hydronium" bars). With the O-protonated pentamethylpenta-dienol ligand present, 2−6 water molecules were observed inside the cage (Figure 3, left, "cation" bars). A representative snapshot showing the substrate with H_3O^+ and three water molecules in the cage is shown on the right-hand side of Figure 3. The hydronium ion shown is poised to protonate the substrate, while other water molecules inside the cage form a H-bond network.
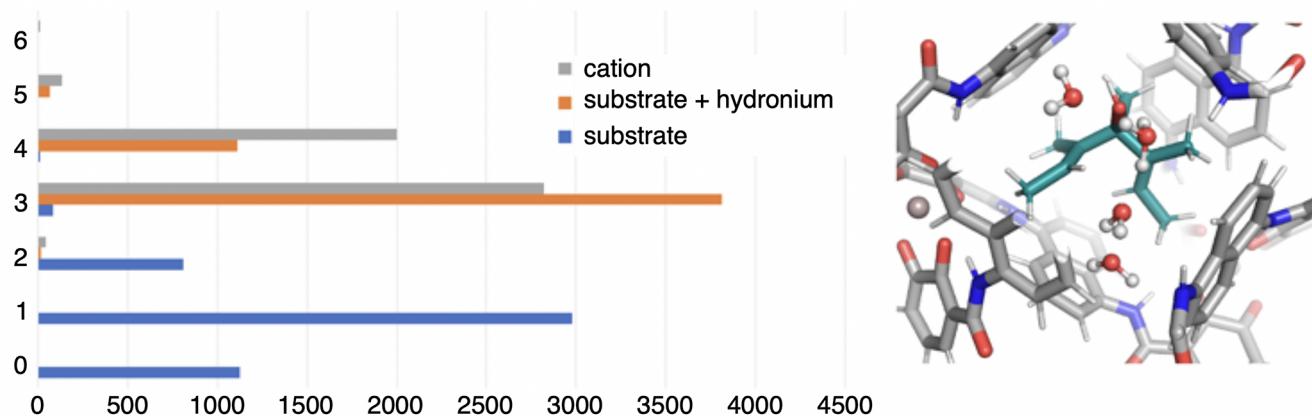
Figure 3. Left: Water molecules inside the cage in MD. Right: Representative snapshot of the substrate with H_3O^+ and three water molecules in the cage (water molecules outside the cage are not shown in this picture for clarity).

Leaving Group Activation—Protonation. We begin by discussing DFT (B3LYP/3-21G-LANL2DZ) results on an encapsulated pentamethylpentadienol substrate (Scheme 1), along with various numbers of water molecules and one H_3O^+ molecule. For these calculations, waters were placed manually near the substrate's hydroxyl group and allowed to relax into the nearest potential energy surface minimum; a consistent solvent configuration was used for all structures. Calculations with different numbers of water molecules and alternative orientations produced qualitatively similar results (see the Supporting Information for details).

First, we focused on the degree to which the substrate protonation event is affected by the Ga_4L_6 cage. To do so, we calculated the free energies associated with protonation of the pentamethylpentadienol reactant inside and outside the cage (both in a water continuum), with various numbers of explicit water molecules present. In all cases, the pentamethylpentadienol reactant was predicted to have a larger (by ≥ 15 kcal/mol) thermodynamic preference for protonation when encapsulated. We also selected configurations from MD simulations using GROMACS clustering with awareness of the symmetry (using RDKit Cookbook) for DFT computations, and for these, encapsulated species are again predicted to be ~15 kcal/mol more basic (see the Supporting Information for details).[21] Warshel and co-workers also argued that the cage interior provides a "remarkable case of a low "local pH","[5a] i.e., encapsulated species are readily protonated. While our computed values here may be overestimates of the pK_a modulation—previous experiments on amine, phosphine, and ester guests indicate that a change in pK_a of 4−5 units, corresponding to 5−7 kcal/mol, can be expected upon encapsulation[10]—it is clear that alcohol basicity is markedly enhanced.

What is the origin of the high acidity of the microenvironment within the Ga_4L_6 cage? The cage used experimentally has walls made of naphthalene rings, and, as shown in Figure 4a, the electrostatic potential within the cage is more negative than that on the cage's outer surface.[22] As a result, it is possible that substrate−cage CH−π interactions strengthen upon protonation, leading to increased substrate basicity.[23] To test the contribution of the cage walls, all naphthalene rings and attached amide groups were removed [and the remaining catechol rings were capped with hydrogen atoms (Figure 4b); note that this does not change the overall charge of the
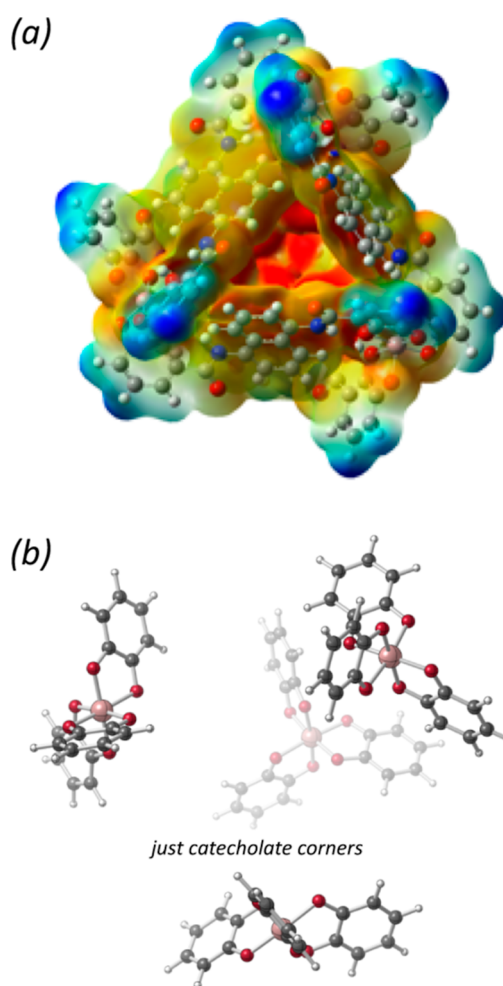

Figure 4. (a) Electrostatic potential surface of the empty cage (isovalue: 0.005, range: −0.83 to −0.5; red is most negative and blue is least negative). (b) Model of the cage with only Ga-catecholate corners.

system], and the substrate protonation energy was recomputed (the geometry of the cage−substrate complex was not allowed to adjust). These changes led to a reduction in predicted protonation energy when no waters are coencapsulated, i.e., protonation is predicted to be less favorable by 17 kcal/mol, consistent with there being interactions between the π-faces of

the cage and the substrate. However, an increase in protonation energy of approximately the same amount is predicted for the complex of the substrate and four bound water molecules, highlighting the fact that some bound waters tend to engage in OH−π interactions that, presumably, decrease the strength of their interactions with the protonated alcohol.

The contributions of specific cage oxygen atoms to basicity modulation were also examined. Keeping the naphthalene walls but deleting all *ortho* catechol oxygen atoms, all *meta* catechol oxygen atoms, or all *ortho* and *meta* oxygen atoms along with all gallium atoms (and capping the remaining aromatic carbons with hydrogen atoms), all changes which lead to a neutral truncated cage, decreased the basicity of the bound substrate, in the absence of bound waters, by approximately 15−20 kcal/mol. This result indicates that both the cage charge and π-rich walls contribute roughly equally to the overall effect in the absence of bound water molecules but are antagonistically coupled.[24] However, in the presence of bound waters, some water molecules will intrude on specific cage−substrate interactions (*vide infra*).

We also examined the proton transfer process using QM/MM calculations. A representative snapshot from our MD simulations is shown in Figure 5 (with the cage removed for
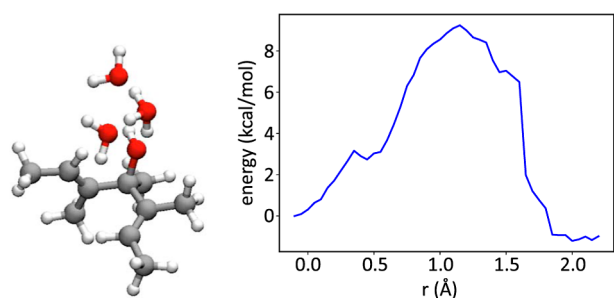

Figure 5. MD snapshot (with the cage and external water molecules removed) and proton transfer scan. r = difference between the substrate C−O bond and the forming O−H bond. The QM region (B3LYP/6-31G*) includes all atoms shown in the structure at left; the MM region includes the cage and a water box (not shown in the figure).

clarity). Note that this structure showcases the general observation that encapsulated waters cluster on one side of the hydrocarbon group as a hydronium ion hydrogen bonds to the substrate hydroxyl group and to two encapsulated waters. When a QM/MM scan of the proton transfer reaction coordinate is carried out, protonated pentamethylpentadienol results (the dip in the energy plot around r = 0.5), which is predicted to be an endothermic process by ∼2.5 kcal/mol, associated with a barrier of ∼3 kcal/mol. For comparison, we examined the protonation of several amines, reported previously to have pK_a's shifted by 4−5 units, using the same approach.[10b] However, little to no barrier was observed computationally in each case, likely because these species are more basic compared to alcohol, precluding meaningful comparisons (see the Supporting Information for details).

Leaving Group Activation—Actually Leaving. What of leaving group loss? Continuing along the scan shown in Figure 5, disconnection of the leaving group inside the cage occurs, resulting in the encapsulated pentamethylpentadienyl cation + 4 H_2O. The barrier for this process is predicted here to be ∼6.5 kcal/mol, somewhat higher than expected. In the absence

of the cage, once the reactant hydroxyl group is protonated, departure of water is expected to occur with little to no barrier. A TSS was not located for this process (modeling such structures is notoriously difficult at best),[25] but a constrained calculation with the breaking bond fixed at 1.9 Å led to a predicted barrier of only 2.5 kcal/mol (note also that in the coiled conformer of O-protonated pentamethylpentadienol, the C−O bond is predicted to be approximately 1.7 Å long). This barrier is similar to the barrier of ∼4 kcal/mol estimated previously for this type of reaction.[2b] Nonetheless, the overall barrier from the alcohol to pentamethylpentadienyl cation is predicted to be significantly lower (reduced by ∼7 kcal/mol) in the cage than in water (blue versus black traces in Figure 6).
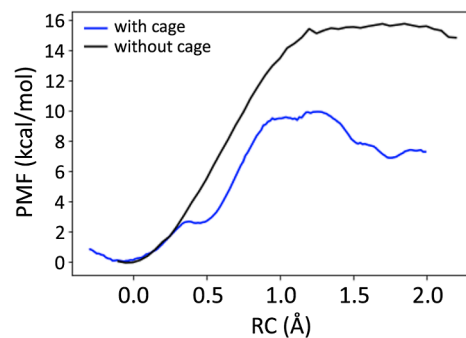

Figure 6. Proton transfer scan (RC = reaction coordinate, which includes both protonation and water disscoiation; PMF = potential mean force) in water and in the cage.

Changing the Cage Vertices—Predictions and Experimental Validation. The barrier to form the pentam-ethylpentadienyl cation is predicted to be 2−3 kcal/mol higher for a cage with Si corners than for a cage with Ga corners (compare Figures 6 and 7), which we ascribe to an electrostatic
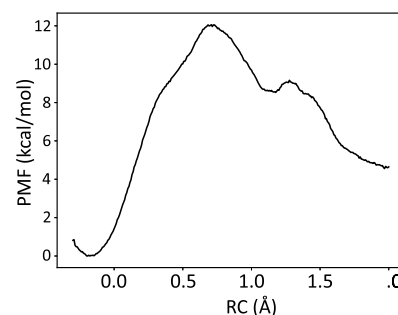

Figure 7. Proton transfer scan for the cage with Si corners (RC = reaction coordinate, which includes both protonation and water disscoiation; PMF = potential mean force) in water and in the cage.

effect that discourages proton transfer to the substrate since that moves positive charge further from the cage corners (see the Supporting Information for additional details). This predicted barrier difference is consistent with the experimental observation of a 680-fold reduction in the rate associated with changing Ga to Si (for **1** with two Z alkenes).[26] If our simple electrostatic model is reasonable, a rate difference also should be observed for the In/Ge pair of catalyst cages but not the Ga/In and Si/Ge pairs.

Synthesis of New Cages. To further confirm the calculated contribution of the charged vertices of the cage to leaving group activation, we sought to compare hosts of

different overall charge and hosts in which the overall charge is maintained but the identity of the metal is changed.

As mentioned above, the metal centers of Ga_4L_6 have previously been replaced to form a catalytically active Si-based host.[26] While it was envisioned that the metal centers could be further diversified to other metals with varied oxidation states, this task presented a major synthetic challenge due to the extreme sensitivity of self-assembly to changes in the structural components. Other catalytically active homogeneous host systems rarely show variability in the metal center.[27] We report here the syntheses of catalytically active Si_4L_6, In_4L_6, and Ge_4L_6 hosts, which were enabled by an optimized and generalizable guest exchange protocol (Figure 8). We then conducted a
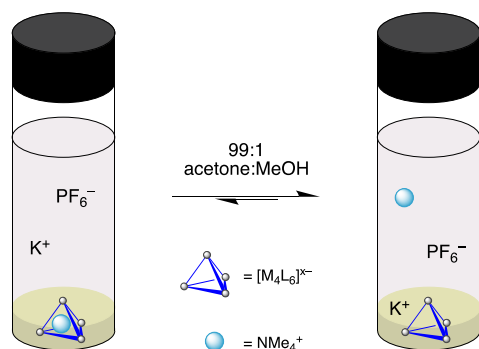

Figure 8. Scheme representing the guest exchange procedure for replacing NMe_4^+ with K^+. M = In(III), Ge(IV), or Si(IV). x = 12, 8, or 8, respectively.

comprehensive experimental study to confirm the structural similarity of these assemblies and determine the contribution of their coordinatively saturated metal centers to supramolecular catalytic reactivity.

We sought to synthesize the In_4L_6 host to provide an isostructural and homo-anionic comparison to Ga_4L_6. The assembly of In_4L_6 was initially probed by combining 6 equiv of ligand L with 4 equiv of indium trisacetylacetonate in the presence of tetraethylammonium bromide, a strongly binding template. The appearance of six aromatic resonances and a diagnostic upfield-shifted guest resonance in the ^1H NMR spectrum confirmed host assembly and encapsulation of the guest (see the Supporting Information). While this was a promising result, a templating guest inhibits host catalysis, and its subsequent removal is hampered by its high association constant. Identifying conditions for a template-free synthesis, however, is often the most challenging step toward accessing

these supramolecular catalysts, given the reduced thermodynamic driving force toward host assembly.

Not surprisingly, the assembly of In_4L_6 was not observed in the absence of a templating guest, even upon prolonged heating at 50 °C in methanol. We thus sought an alternative approach, where a weakly binding cationic template such as tetramethylammonium could be used to first enable self-assembly and subsequently be displaced by potassium counterions to expose the catalytically active host cavity. The guest exchange relies on a large excess of potassium ions to drive the binding equilibrium toward a K^+-associated host, effectively overcoming the higher association constant of the cationic template. This approach has been previously employed for $NMe_4^+ \subset Ga_4L_6$, which resulted in relatively poor recovery (36−41% yield) due to the similar solubility profiles of the host and excess KI (the K^+ source).[27,28]

Fortunately, the assembly of $NMe_4^+ \subset In_4L_6$ was observed in the presence of a superstoichiometric amount of tetramethylammonium bromide. Subjecting $NMe_4^+ \subset In_4L_6$ to guest exchange conditions identical to those used for Ga_4L_6, however, afforded only a trace yield (<5%) of K^+-associated In_4L_6, prompting an extensive screening to identify conditions for a better protocol. Ultimately, stirring $NMe_4^+ \subset In_4L_6$ in a saturated solution of KPF_6 in acetone and a small amount of methanol overnight yielded optimal exchange and recovery (Figure 8). Differences in solubility between the host and excess KPF_6 under the reaction conditions enabled nearly quantitative recovery of In_4L_6 by filtration, and after five repeated iterations of the exchange protocol, less than 0.1 equiv of tetramethylammonium remained, as confirmed by ^1H NMR spectroscopy (after two rounds of guest exchange, less than 0.2 equiv of NMe_4^+ remained, yielding a catalytically active host). The stoichiometry and overall charge of In_4L_6 were further verified by electrospray ionization mass spectrometry (ESI-MS), where it was primarily detected in the 3^- and 4^- charge states with various counterions. Compared to the Ga_4L_6 analogue, In_4L_6 shows an increased sensitivity to oxidation and other decomposition pathways, which was evidenced by rapid attenuation of the signal on ESI-MS.

Next, we turned to the synthesis of Ge_4L_6, which we hoped would provide an isostructural and homo-anionic comparison to Si_4L_6. While the template-free assembly of Ge_4L_6 was not observed, $NMe_4^+ \subset Ge_4L_6$ could be formed by heating 6 equiv of the ligand and 4 equiv of Ge(IV) methoxide in dimethylformamide in the presence of 5 equiv of NMe_4Br. $NMe_4^+ \subset Ge_4L_6$ was subjected to the modified guest exchange
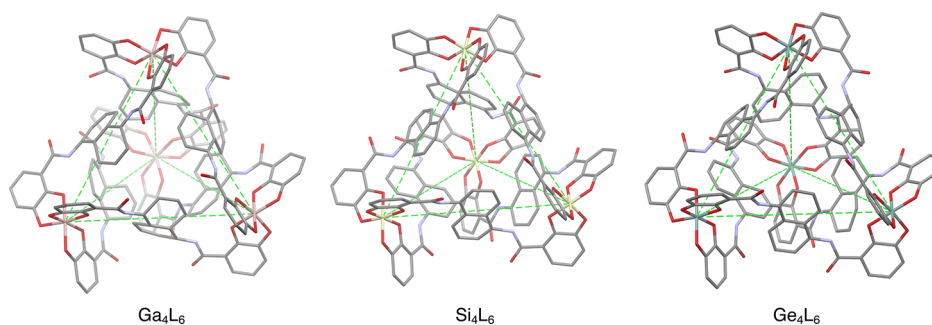

Figure 9. Structures obtained by SCXRD of Ga_4L_6, Si_4L_6, and Ge_4L_6. Metal−metal distances are highlighted in green. For Ga_4L_6, the average Ga−Ga distance is 12.663(3) Å and the volume is 239.3(1) Å^3. For Si_4L_6, the average Si−Si distance is 12.655(2) Å and the volume is 238.85(6) Å^3. For Ge_4L_6, the average Ge−Ge distance is 12.717(3) Å and the volume is 242.39(4) Å^3.

conditions which afforded K^+-associated Ge_4L_6, albeit in lower yields. This decrease in yield was attributed to differences in solubility of In_4L_6 and Ge_4L_6: the lower 8^- charge enhances the solubility of Ge_4L_6 in organic solvents such as acetone while slightly decreasing its water solubility. Gratifyingly, addition of a small amount (1 mL) of water to the saturated KPF_6 solution in acetone resulted in the quantitative recovery of Ge_4L_6, which was characterized by ^{1}H NMR spectroscopy and ESI-MS, detected in the 4^- and 5^- charge states.

While the template-free synthesis of Si_4L_6 has been shown, it required elevated temperatures, long reaction times (60 h), and rigorous purification. We envisioned that applying the guest exchange protocol would not only serve as a proof-of-concept for the general applicability of the method but could also enable assembly under milder conditions. Indeed, $NMe_4^+ \subset Si_4L_6$ was quantitatively formed after just 16 h, and guest exchange conditions afforded clean $Si_4L_6/K+$, which could be used without further purification.

Structural data obtained by single crystal X-ray diffraction (SCXRD) confirmed that the cavity size and metal−metal distances were very similar between Ga_4L_6, Si_4L_6, and Ge_4L_6. The crystals of $NEt_4^+ \subset Ge_4L_6$ were grown by vapor diffusion of benzene into a solution in dimethyl sulfoxide and measured with synchrotron radiation. Like Ga_4L_6 and Si_4L_6, Ge_4L_6 is an ideal tetrahedron, with an average edge length of 12.717(3) Å and a volume of 242.39(4) Å^3 (Figure 9). Although we could not obtain SCXRD measurements for In_4L_6, we can expect similarly small deviations in the size and structure of the host as the difference in metal−oxygen bond lengths between these four elements (Ga, Si, Ge, and In) is small (<0.5 Å) compared to the edge length of the tetrahedron. These data demonstrate that the metal−ligand coordination environment is well-preserved between the hosts, confirming their isostructural relationship in the solid state.

In contrast, the total fluorescence yield from the O K-edge soft X-ray absorption spectroscopy (sXAS) data of the four hosts (recorded on BL8.0.1 at the ALS) is shown in Figure 10. Because all the meta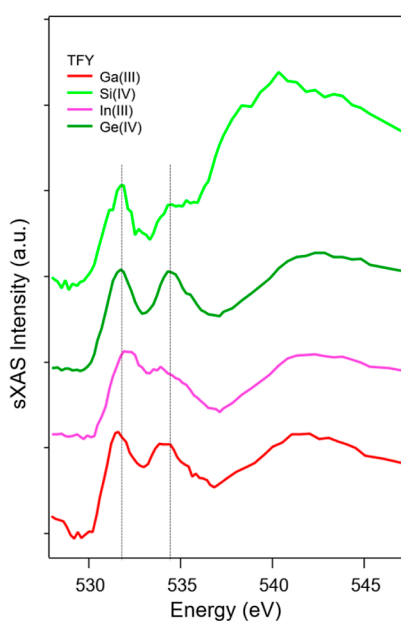l ions have filled d manifolds, the pre-edge features of the O K-edge sXAS (between 530 and 535 eV) mainly reflect the transitions from O 1s orbitals to the empty orbitals near the lowest unoccupied molecular orbital (LUMO) with O p characters.[29,30] The differences in energy splitting and relative intensities imply different electronic structures of the LUMOs, although they all have similar geometric structures. The existence of such differences is supported by the varied assembly conditions that were required when the metal vertices were changed.

Catalytic Rates. With these four isostructural assemblies consisting of two homo-anionic pairs (12^- and 8^-) in hand, we sought to compare their catalytic activity and observe the effect of changing the metal vertices on the host-catalyzed Nazarov cyclization. Our aim was to determine whether the structural similarity between the hosts would induce similar catalytic behavior or if the electronic differences in metal−oxygen binding would cause divergence. Previous comparison of the Ga_4L_6- and Si_4L_6-catalyzed aza-Cope rearrangement, which proceeds with retention of the cationic charge on the substrate and is driven primarily by constrictive binding within the host, exhibited rates of reaction within error of each other. In_4L_6 and Ge_4L_6 were also shown to catalyze the aza-Cope rearrangement at similar rates to Ga_4L_6 and Si_4L_6, further confirming that structurally similar hosts show no difference in reactivity for a reaction that is not sensitive to changes in host charge (see the Supporting Information). In contrast, the Nazarov cyclization is initiated by protonation of a neutral dienol substrate, resulting in an overall increase in cationic charge within the host microenvironment. Comparison of the Ga_4L_6 and Si_4L_6 catalysts demonstrated a 680-fold difference in rate acceleration, implying that the reaction is indeed sensitive to the host charge.[26] Further investigation of the In_4L_6- and Ge_4L_6-catalyzed reactions should thus enable us to probe the extent to which the identity of the metal affects charge-based supramolecular catalytic reactivity and validate whether the substitution of Al for Ga and Si in the computational model is appropriate.

We investigated the Nazarov cyclization of dienol **1** (with two Z alkenes), which previously demonstrated sensitivity to changes in overall host charge (Scheme 1).[26] Due to the large discrepancy in the rate of the Ga_4L_6- and Si_4L_6-catalyzed reactions, kinetic data were previously obtained at different temperatures and extrapolated for comparison using an Eyring analysis. The In_4L_6-catalyzed reaction could be monitored over the course of a few hours at 45 °C, while the Ge_4L_6-catalyzed reaction required heating to 72 °C to measure the reaction rate on a practicable experimental timescale. This initial observation led us to investigate the four hosts as homo-anionic pairs, where the Ga_4L_6- and In_4L_6-catalyzed reactions were compared at 45 °C, and Si_4L_6- and Ge_4L_6-catalyzed reactions were compared at 72 °C (Table 1).

Figure 10. Oxygen K-edge sXAS data of Ga_4L_6, Si_4L_6, In_4L_6, and Ge_4L_6.

Table 1. Rate Constants (k_{obs}) for the Host-Catalyzed Nazarov Cyclization

Catalyst	Catalyst Loading (%)	Temperature	k_{obs} (s^{-1})
$[Ga_4L_6]^{12-}$	7%	45 °C	4.2(3)×10^{-4}
$[In_4L_6]^{12-}$	10%	45 °C	8.3(1)×10^{-4}
$[Si_4L_6]^{8-}$	7%	72 °C	2.2(4)×10^{-4}
$[Ge_4L_6]^{8-}$	6%	72 °C	1.7(1)×10^{-4}

Though the host–dienol Michaelis complex is clearly observable by ^{1}H NMR spectroscopy, encapsulation is not quantitative due to the high dissociation constant (K_d) of the neutral alcohol substrate. While substrate-dependence studies have not been conducted for the host-catalyzed Nazarov cyclization, it is reasonable to assume that the reaction is not in the saturation regime under these conditions. Thus, the first-order k_{obs} is dependent on the value of the Michaelis constant (K_m), which can be approximated by K_d. Because small hydrocarbon molecules are encapsulated by the hydrophobic effect, rather than Coulombic attraction, their association is driven primarily by entropic effects.[31] Because of this, we expect a negligible difference in K_d of **1** between the two hosts as the host charge plays a minimal role as a driving force for association.

Evidently, the discrepancies in the reaction rates based on the host charge reaffirms the ability of the metal centers to impact catalysis by imparting an overall charge on the host assembly. However, the close agreement in rates between the respective tri- and tetravalent metal centers provides evidence that key electrostatic interactions between the host and the transition state are not significantly perturbed between different homo-cationic metals, consistent with the calculated predictions. These experimental comparisons enable us to pinpoint the specific role of the metal center in catalysis, despite the complexity of structure–activity relationships in multicomponent, self-assembled systems.

The development of an efficient guest exchange protocol enabled high-yielding syntheses of catalytically active Si_4L_6, In_4L_6, and Ge_4L_6 supramolecular hosts. Together with Ga_4L_6, these isostructural catalysts enabled an extensive experimental investigation to isolate the effects of the metal center, an important structural component, on catalytic reactivity. All hosts demonstrated similar catalytic ability for the constrictive-binding-driven aza-Cope rearrangement regardless of the identity or oxidation state of the metal center. While In_4L_6 and Ge_4L_6 hosts demonstrated significant discrepancies in the rate ($k_{obs} = 8.3 \times 10^{-4}$ s^{-1} at 45 °C vs 1.7×10^{-4} s^{-1} at 72 °C) for the Nazarov cyclization, reactivity was comparable between hosts with homo-cationic metal centers, in agreement with predictions. These results imply that the structural similarity between the hosts determined their similar catalytic behavior, outweighing the differences in electronic structures implied by the LUMOs with O p characters indicated by the sXAS data.

Overall Model. Thus, we arrive at the following model for rate acceleration. Protonation of the reactant alcohol is greatly enhanced upon complexation, leading to a large net acceleration of water loss. Electrocyclization may be enhanced but only slightly. Warshel and co-workers similarly concluded that selective transition state stabilization was much less significant than reactant protonation for an orthoformate hydrolysis reaction promoted by the Ga_4L_6 cage.[5a,10a]

Evidence continues to mount that the reactivity of carbocations generated in the active sites of terpene synthases reflects their energetics in the gas phase.[1d] This was predicted on the basis of results of quantum chemical computations, and multiple experiments with enzymatic systems support this model.[32] Here, we have shown that a very similar scenario occurs for the Ga_4L_6 cage; the cage facilitates formation of a pentadienyl carbocation, but barrier lowering is not at all necessary for the cyclization reaction step. While type 1 terpene synthase enzymes activate their substrates' leaving groups (diphosphate groups) primarily by binding to Lewis

acidic magnesium ions,[1a] the Ga_4L_6 cage activates its substrates' leaving groups *via* facilitation of protonation. Protonation is also used in other (type 2) terpene synthases to generate carbocations from epoxides or alkenes.[33] In addition to utilizing active-site amino acid sidechains with enhanced acidity (resulting from hydrogen-bonding arrays in which they participate), these terpene synthases provide active site cavities that interact favorably with the carbocations generated upon protonation. Like the Ga_4L_6 cage, these active sites are lined with aromatic amino acid sidechains that can participate in carbocation–π interactions;[3d,22,34] however, the cage also appears to bind to several water molecules along with the substrate.[5b,c] While waters do sometimes bind along with substrates for terpene synthases, they tend to be fewer in number.

■ CONCLUSIONS

Supramolecular catalysis systems remain challenging to model due to the large number of atoms involved and the significant influence of noncovalent and solvent interactions. Our work shows agreement between calculation and experimental data on structure–activity relationships, a promising example of the computational modeling of a complex supramolecular system.

■ ASSOCIATED CONTENT

⑤ Supporting Information

The Supporting Information is available free of charge at https://pubs.acs.org/doi/10.1021/jacs.2c04179.

> Details of computational methods and structures; general procedures, synthesis, and characterization of compounds; general procedures for kinetics experiments; representative spectra and kinetics data; ESI-MS data; crystallographic analysis of Ge_4L_6; and ^{1}H NMR spectra (PDF)

Accession Codes

CCDC 2088585 contains the supplementary crystallographic data for this paper. These data can be obtained free of charge via www.ccdc.cam.ac.uk/data_request/cif, or by emailing data_request@ccdc.cam.ac.uk, or by contacting The Cambridge Crystallographic Data Centre, 12 Union Road, Cambridge CB2 1EZ, UK; fax: +44 1223 336033.

■ AUTHOR INFORMATION

Corresponding Authors

Robert G. Bergman — *Department of Chemistry, University of California, Berkeley, California 94720, United States; Chemical Sciences Division, Lawrence Berkeley National Laboratory, Berkeley, California 94720, United States;* ⓘ orcid.org/0000-0002-3105-8366; Email: rbergman@berkeley.edu

Kenneth N. Raymond — *Department of Chemistry, University of California, Berkeley, California 94720, United States; Chemical Sciences Division, Lawrence Berkeley National Laboratory, Berkeley, California 94720, United States;* Email: raymond@socrates.edu

F. Dean Toste — *Department of Chemistry, University of California, Berkeley, California 94720, United States; Chemical Sciences Division, Lawrence Berkeley National Laboratory, Berkeley, California 94720, United States;* ⓘ orcid.org/0000-0001-8018-2198; Email: fdtoste@berkeley.edu

Dean J. Tantillo − *Department of Chemistry, University of California, Davis, Davis, California 95616, United States;* ⊙ orcid.org/0000-0002-2992-8844; Email: djtantillo@ucdavis.edu

Authors

Quynh Nhu N. Nguyen − *Department of Chemistry, University of California, Davis, Davis, California 95616, United States*

Kay T. Xia − *Department of Chemistry, University of California, Berkeley, California 94720, United States; Chemical Sciences Division, Lawrence Berkeley National Laboratory, Berkeley, California 94720, United States*

Yue Zhang − *Department of Chemistry, University of California, Davis, Davis, California 95616, United States;* ⊙ orcid.org/0000-0003-4142-3723

Nanhao Chen − *Department of Chemistry, University of California, Davis, Davis, California 95616, United States*

Mariko Morimoto − *Department of Chemistry, University of California, Berkeley, California 94720, United States; Chemical Sciences Division, Lawrence Berkeley National Laboratory, Berkeley, California 94720, United States;* ⊙ orcid.org/0000-0001-8084-1042

Xiaokun Pei − *Department of Chemistry, University of California, Berkeley, California 94720, United States;* ⊙ orcid.org/0000-0002-6074-1463

Yang Ha − *Advanced Light Source, Lawrence Berkeley National Laboratory, Berkeley, California 94720, United States*

Jinghua Guo − *Advanced Light Source, Lawrence Berkeley National Laboratory, Berkeley, California 94720, United States;* ⊙ orcid.org/0000-0002-8576-2172

Wanli Yang − *Advanced Light Source, Lawrence Berkeley National Laboratory, Berkeley, California 94720, United States;* ⊙ orcid.org/0000-0003-0666-8063

Lee-Ping Wang − *Department of Chemistry, University of California, Davis, Davis, California 95616, United States;* ⊙ orcid.org/0000-0003-3072-9946

Complete contact information is available at:
https://pubs.acs.org/10.1021/jacs.2c04179

◼ REFERENCES

(1) (a) Christianson, D. W. Structural Biology and Chemistry of the Terpenoid Cyclases. *Chem. Rev.* **2006**, *106*, 3412−3442. (b) Christianson, D. W. Unearthing the Roots of the Terpenome. *Curr. Opin. Chem. Biol.* **2008**, *12*, 141−150. (c) Tantillo, D. J. Biosynthesis via carbocations: Theoretical studies on terpene formation. *Nat. Prod. Rep.* **2011**, *28*, 1035−1053. (d) Tantillo, D. J. Importance of Inherent Substrate Reactivity in Enzyme-Promoted Carbocation Cyclization/Rearrangements. *Angew. Chem., Int. Ed.* **2017**, *56*, 10040−10045.

(2) (a) Hastings, C. J.; Pluth, M. D.; Bergman, R. G.; Raymond, K. N. Enzymelike Catalysis of the Nazarov Cyclization by Supramolecular Encapsulation. *J. Am. Chem. Soc.* **2010**, *132*, 6938−6940. (b) Hastings, C. J.; Bergman, R. J.; Raymond, K. N. Origins of Large Rate Enhancements in the Nazarov Cyclization Catalyzed by Supramolecular Encapsulation. *Chem.—Eur. J.* **2014**, *20*, 3966−3973.

(3) Representative examples: (a) Pronin, S. V.; Shenvi, R. A. Synthesis of highly strained terpenes by non-stop tail-to-head polycyclization. *Nat. Chem.* **2012**, *4*, 915−920. (b) Zhang, Q.; Tiefenbacher, K. Terpene cyclization catalysed inside a self-assembled cavity. *Nat. Chem.* **2015**, *7*, 197−202. (c) Geier, M. J.; Gagné, M. R. Diastereoselective Pt Catalyzed Cycloisomerization of Polyenes to Polycycles. *J. Am. Chem. Soc.* **2014**, *136*, 3032−3035. (d) Kennedy, C. R.; Lin, S.; Jacobsen, E. N. The Cation−π Interaction in Small-Molecule Catalysis. *Angew. Chem., Int. Ed.* **2016**, *55*, 12596−12624. (e) Zhang, Q.; Catti, L.; Pleiss, J.; Tiefenbacher, K. Terpene Cyclizations inside a Supramolecular Catalyst: Leaving-Group-Controlled Product Selectivity and Mechanistic Studies. *J. Am. Chem. Soc.* **2017**, *139*, 11482−11492.

(4) (a) Hare, S. R.; Tantillo, D. J. Dynamic Behavior of Rearranging Carbocations − Implications for Terpene Biosynthesis. *Beilstein J. Org. Chem.* **2016**, *12*, 377−390. (b) Tantillo, D. J. Exploring Terpenoid Biosynthesis with Quantum Chemical Computations. *Compr. Nat. Prod. III* **2020**, *1*, 644−653.

(5) (a) Frushicheva, M. P.; Mukherjee, S.; Warshel, A. Electrostatic Origin of the Catalytic Effect of a Supramolecular Host Catalyst. *J. Phys. Chem. B* **2012**, *116*, 13353−13360. (b) Norjmaa, G.; Maréchal, J.-D.; Ujaque, G. Microsolvation and Encapsulation Effects on Supramolecular Catalysis: C−C Reductive Elimination inside $[Ga_4L_6]^{12-}$ Metallocage. *J. Am. Chem. Soc.* **2019**, *141*, 13114−13123. (c) Norjmaa, G.; Maréchal, J.-D.; Ujaque, G. Reaction Rate Inside the Cavity of $[Ga_4L_6]^{12-}$ Supramolecular Metallocage is Regulated by the Encapsulated Solvent. *Chem.—Eur. J.* **2020**, *26*, 6988−6992. (d) Norjmaa, G.; Maréchal, J.-D.; Ujaque, G. Origin of the Rate Acceleration in the C-C Reductive Elimination from Pt(IV)-complex in a $[Ga_4L_6]^{12-}$ Supramolecular Metallocage. *Chem.—Eur. J.* **2021**, *27*, 15973−15980. (e) Sebastiani, F.; Bender, T. A.; Pezzotti, S.; Li, W.-L.; Schwaab, G.; Bergman, R. G.; Raymond, K. N.; Toste, F. D.; Head-Gordon, T.; Havenith, M.; Havenith, M. An isolated water droplet in the aqueous solution of a supramolecular tetrahedral cage. *Proc. Natl. Acad. Sci. U.S.A.* **2020**, *117*, 32954−32961. (f) Li, W.-L.; Hao, H.; Head-Gordon, T. Optimizing the Solvent Reorganization Free Energy by Metal Substitution for Nanocage Catalysis. *ACS Catal.* **2022**, *12*, 3782−3788.

(6) Ronson, T. K.; League, A. B.; Gagliardi, L.; Cramer, C. J.; Nitschke, J. R. Pyrene-Edged FeII4L6 Cages Adaptively Reconfigure During Guest Binding. *J. Am. Chem. Soc.* **2014**, *136*, 15615−15624.

(7) (a) Becke, A. D. Density-functional thermochemistry. III. The role of exact exchange. *J. Chem. Phys.* **1993**, *98*, 5648−5652. (b) Becke, A. D. A new mixing of Hartree−Fock and local density-functional theories. *J. Chem. Phys.* **1993**, *98*, 1372−1377. (c) Lee, C.;

Yang, W.; Parr, R. G. Development of the Colle-Salvetti correlation-energy formula into a functional of the electron density. *Phys. Rev. B* **1988**, *37*, 785−789. (d) Stephens, P. J.; Devlin, F. J.; Chabalowski, C. F.; Frisch, M. J. Ab Initio Calculation of Vibrational Absorption and Circular Dichroism Spectra Using Density Functional Force Fields. *J. Phys. Chem.* **1994**, *98*, 11623−11627.

(8) Hay, P. J.; Wadt, W. R. *Ab initio* effective core potentials for molecular calculations. Potentials for the transition metal atoms Sc to Hg. *J. Chem. Phys.* **1985**, *82*, 270−283.

(9) Tomasi, J.; Mennucci, B.; Cammi, R. Quantum Mechanical Continuum Solvation Models. *Chem. Rev.* **2005**, *105*, 2999−3094.

(10) (a) Pluth, M. D.; Bergman, R. G.; Raymond, K. N. Acid catalysis in basic solution: a supramolecular host promotes orthoformate hydrolysis. *Science* **2007**, *316*, 85−88. (b) Pluth, M. D.; Bergman, R. G.; Raymond, K. N. Making amines strong bases: thermodynamic stabilization of protonated guests in a highly-charged supramolecular host. *J. Am. Chem. Soc.* **2007**, *129*, 11459−11467.

(11) Wang, J.; Wolf, R. M.; Caldwell, J. W.; Kollman, P. A.; Case, D. A. Development and Testing of a General Amber Force Field. *J. Comput. Chem.* **2004**, *25*, 1157−1174.

(12) Bayly, C. I.; Cieplak, P.; Cornell, W.; Kollman, P. A. A Well-Behaved Electrostatic Potential Based Method Using Charge Restraints for Deriving Atomic Charges: The RESP Model. *J. Phys. Chem.* **1993**, *97*, 10269−10280.

(13) Case, D. A.; Betz, R. M.; Cerutti, D. S.; Cheatham, T. E.; Darden, T.; Duke, R. E. *AMBER 16*, 2016: San Francisco.

(14) Andersen, H. C. A "Velocity" Version of the Shake Algorithm for Molecular Dynamics Calculations. *J. Comput. Phys.* **1983**, *52*, 24−34.

(15) Essmann, U.; Perera, L.; Berkowitz, M. L.; Darden, T.; Lee, H.; Pedersen, L. G. A Smooth Particle Mesh Ewald Method. *J. Chem. Phys.* **1995**, *103*, 8577−8593.

(16) Eastman, P.; Swails, J.; Chodera, J. D.; McGibbon, R. T.; Zhao, Y.; Beauchamp, K. A.; Wang, L.-P.; Simmonett, A. C.; Harrigan, M. P.; Stern, C. D.; Wiewiora, R. P.; Brooks, B. R.; Pande, V. S. OpenMM 7: Rapid Development of High Performance Algorithms for Molecular Dynamics. *PLoS Comput. Biol.* **2017**, *13*, No. e1005659.

(17) (a) Zhou, Y.; Wang, S.; Li, Y.; Zhang, Y. Born−Oppenheimer Ab Initio QM/MM Molecular Dynamics Simulations of Enzyme Reactions. *Methods Enzymol.* **2016**, *577*, 105−118. (b) Shao, Y.; Gan, Z.; Epifanovsky, E.; Gilbert, A. T. B.; Wormit, M.; Kussmann, J.; Lange, A. W.; Behn, A.; Deng, J.; Feng, X.; et al. Advances in molecular quantum chemistry contained in the Q-Chem 4 program package. *Molecular Physics* **2015**, *113*, 184.

(18) Souaille, M.; Roux, B. Extension to the Weighted Histogram Analysis Method: Combining Umbrella Sampling with Free Energy Calculations. *Comput. Phys. Commun.* **2001**, *135*, 40−57.

(19) Chai, J.-D.; Head-Gordon, M. Long-range corrected hybrid density functionals with damped atom−atom dispersion corrections. *Phys. Chem. Chem. Phys.* **2008**, *10*, 6615−6620.

(20) The structures of water clusters are still actively studied, e.g. Wolke, C. T.; Fournier, J. A.; Dzugan, L. C.; Fagiani, M. R.; Odbadrakh, T. T.; Knorke, H.; Jordan, K. D.; McCoy, A. B.; Asmis, K. R.; Johnson, M. A. Spectroscopic snapshots of the proton-transfer mechanism in water. *Science* **2016**, *354*, 1131−1135.

(21) Lindahl, A.; van der Hess, S. *GROMACS*; Zenodo, 2021; Vol. *4*. Manual (2021.4).

(22) Klärner, F.-G.; Panitzky, J.; Preda, D.; Scott, L. T. Modeling of Supramolecular Properties of Molecular Tweezers, Clips, and Bowls. *Mol. Model Ann.* **2000**, *6*, 318−327.

(23) Dougherty, D. A. Cation-π Interactions in Chemistry and Biology: A New View of Benzene, Phe, Tyr, and Trp. *Science* **1996**, *271*, 163−168.

(24) Wheeler, S. E. Understanding Substituent Effects in Noncovalent Interactions Involving Aromatic Rings. *Acc. Chem. Res.* **2013**, *46*, 1029−1038.

(25) (a) Schreiner, P. R.; Schleyer, P. v. R.; Schaefer, H. F. Why the Classical and Nonclassical Norbornyl Cations Do Not Resemble the 2-*endo*- and 2-*exo*-Norbornyl Solvolysis Transition States. *J. Org. Chem.* **1997**, *62*, 4216−4228. (b) Byrne, P. A.; Kobayashi, S.; Würthwein, E.-U.; Ammer, J.; Mayr, H. Why Are Vinyl Cations Sluggish Electrophiles? *J. Am. Chem. Soc.* **2017**, *139*, 1499−1511.

(26) Hong, C. M.; Morimoto, M.; Kapustin, E. A.; Alzakhem, N.; Bergman, R. G.; Raymond, K. N.; Toste, F. D. Deconvoluting the Role of Charge in a Supramolecular Catalyst. *J. Am. Chem. Soc.* **2018**, *140*, 6591−6595.

(27) The Fujita M_6L_4 host represents a notable exception, where isostructural Pd(II) and Pt(II)-based analogues have been synthesized. (See: (a) Ibukuro, F.; Kusukawa, T.; Fujita, M. A Thermally Switchable Molecular Lock. Guest-Templated Synthesis of a Kinetically Stable Nanosized Cage. *J. Am. Chem. Soc.* **1998**, *120*, 8561−8562. (b) Fujita, M.; Umemoto, K.; Yoshizawa, M.; Fujita, N.; Kusukawa, T.; Biradha, K. Molecular Paneling via Coordination. *Chem. Commun.* **2001**, *6*, 509−518. (c) Fujita, M.; Oguro, D.; Miyazawa, M.; Oka, H.; Yamaguchi, K.; Ogura, K. Self-Assembly of Ten Molecules into Nanometre-Sized Organic Host Frameworks. *Nature* **1995**, *378*, 469−471. However, while there is ample precedent for supramolecular catalysis using the Pd(II)-based host, (See (d) Yoshizawa, M.; Klosterman, J. K.; Fujita, M. Functional Molecular Flasks: New Properties and Reactions within Discrete, Self-Assembled Hosts. *Angew. Chem., Int. Ed.* **2009**, *48*, 3418−3438. (e) Fujita, M.; Yoshizawa, M. New Properties and Reactions in Self-Assembled M6L4 Coordination Cages. *Modern Supramolecular Chemistry*; John Wiley & Sons, Ltd, 2008; pp 277−313. (f) Yoshizawa, M.; Miyagi, S.; Kawano, M.; Ishiguro, K.; Fujita, M. Alkane Oxidation via Photochemical Excitation of a Self-Assembled Molecular Cage. *J. Am. Chem. Soc.* **2004**, *126*, 9172−9173. (g) Takezawa, H.; Kanda, T.; Nanjo, H.; Fujita, M. Site-Selective Functionalization of Linear Diterpenoids through U-Shaped Folding in a Confined Artificial Cavity. *J. Am. Chem. Soc.* **2019**, *141*, 5112−5115. (h) Yoshizawa, M.; Tamura, M.; Fujita, M. Diels-Alder in Aqueous Molecular Hosts: Unusual Regioselectivity and Efficient Catalysis. *Science* **2006**, *312*, 251−254. catalysis using the Pt(II)-based host was only recently reported (See (i) Takezawa, H.; Shitozawa, K.; Fujita, M. Enhanced Reactivity of Twisted Amides inside a Molecular Cage. *Nat. Chem.* **2020**, *12*, 574−578. In this recent example, differences in stability between the two hosts precluded a direct comparison of their catalytic abilities (only the Pt(II)-based host was viable for catalysis), leaving the specific effects of the metal centers ambiguous

(28) Davis, A. V.; Fiedler, D.; Ziegler, M.; Terpin, A.; Raymond, K. N. Resolution of Chiral, Tetrahedral M_4L_6 Metal−Ligand Hosts1. *J. Am. Chem. Soc.* **2007**, *129*, 15354−15363.

(29) Sánchez-de-Armas, R.; San-Miguel, M. A.; Oviedo, J.; Márquez, A.; Sanz, J. F. Electronic structure and optical spectra of catechol on TiO2 nanoparticles from real time TD-DFT simulations. *Phys. Chem. Chem. Phys.* **2011**, *13*, 1506−1514.

(30) Tenderholt, A. L.; Szilagyi, R. K.; Holm, R. H.; Hodgson, K. O.; Hedman, B.; Solomon, E. I. Electronic Control of the "Bailar Twist" in Formally d0-d2 Molybdenum Tris(dithiolene) Complexes: A Sulfur K-edge X-ray Absorption Spectroscopy and Density Functional Theory Study. *Inorg. Chem.* **2008**, *47*, 6382−6392.

(31) (a) Leung, D. H.; Bergman, R. G.; Raymond, K. N. Enthalpy-Entropy Compensation Reveals Solvent Reorganization as a Driving Force for Supramolecular Encapsulation in Water. *J. Am. Chem. Soc.* **2008**, *130*, 2798−2805. (b) Sebastiani, F.; Bender, T. A.; Pezzotti, S.; Li, W.-L.; Schwaab, G.; Bergman, R. G.; Raymond, K. N.; Toste, F. D.; Head-Gordon, T.; Havenith, M. An Isolated Water Droplet in the Aqueous Solution of a Supramolecular Tetrahedral Cage. *Proc. Natl. Acad. Sci. U.S.A.* **2020**, *117*, 32954−32961.

(32) Representative examples (a) Zu, L.; Xu, M.; Lodewyk, M. W.; Cane, D. E.; Peters, R. J.; Tantillo, D. J. Effect of Isotopically Sensitive Branching on Product Distribution for Pentalenene Synthase: Support for a Mechanism Predicted by Quantum Chemistry. *J. Am. Chem. Soc.* **2012**, *134*, 11369−11371. (b) Jackson, A. J.; Hershey, D. M.; Chesnut, T.; Xu, M.; Peters, R. J. Biochemical characterization of the castor bean ent-kaurene synthase(-like) family supports quantum chemical view of diterpene cyclizatio. *Phytochem* **2014**, *103*, 13−21. (c) Sato, H.; Teramoto, K.; Masumoto, Y.; Tezuka, N.; Sakai, K.;

Ueda, S.; Totsuka, Y.; Shinada, T.; Nishiyama, M.; Wang, C.; Kuzuyama, T.; Uchiyama, M. Cation-Stitching Cascade": exquisite control of terpene cyclization in cyclooctatin biosynthesis. *Sci. Rep.* **2015**, *5*, 18471. (d) Dickschat, J. S.; Brock, N. L.; Citron, C. A.; Tudzynski, B. Biosynthesis of Sesquiterpenes by the Fungus *Fusarium verticillioides. ChemBioChem* **2011**, *12*, 2088−2095. (e) Rinkel, J.; Rabe, P.; Garbeva, P.; Dickschat, J. S. Lessons from 1,3-Hydride Shifts in Sesquiterpene Cyclizations. *Angew. Chem., Int. Ed.* **2016**, *55*, 13593−13596.

(33) Abe, I.; Rohmer, M.; Prestwich, G. D. Enzymatic cyclization of squalene and oxidosqualene to sterols and triterpenes. *Chem. Rev.* **1993**, *93*, 2189−2206.

(34) (a) Hong, Y. J.; Tantillo, D. J. Tension between Internal and External Modes of Stabilization in Carbocations Relevant to Terpene Biosynthesis - Modulating Minima Depth via C−H●●●π Interactions. *Org. Lett.* **2015**, *17*, 5388−5391. (b) Hong, Y. J.; Tantillo, D. J. C-H●●●π Interactions as Modulators of Carbocation Structure - Implications for Terpene Biosynthesis. *Chem. Sci.* 2013, *4*, 2512-2518. DOI: 10.1039/c3sc50571e